Time-dependent second order scattering theory for a weather radar with a finite beam width

Satoru Kobayashi
Simone Tanelli
and Eastwood Im
Jet Propulsion Laboratory
California Institute of Technology
Pasadena, California, 91101
Email: Satoru.Kobayashi@jpl.nsa.gov

Shigeo Ito
Toyo University
Kawagoe, Saitama, Japan
Email: ito@eng.toyo.ac.jp

Tomohiro Oguchi
Kanto Gakuin University
Yokohama, Kanagawa, Japan
r-oguchi@js.ejnet.ne.jp

***Abstract*— Multiple scattering effects from spherical water particles of uniform diameter are studied for a W-band pulsed radar. The Gaussian transverse beam-profile and the rectangular pulse-duration are used for calculation. An second-order analytical solution is derived for a single layer structure, based on a time-dependent radiative transfer theory as described in the authours' companion paper. When the range resolution is fixed, increase in footprint radius leads to increase in the second order reflectivity that is defined as the ratio of the second order return to the first order one. This feature becomes more serious as the range increases. Since the spaceborne millimeter-wavelength radar has a large footprint radius that is competitive to the mean free path, the multiple scattering effect must be taken into account for analysis.**

I. Introduction

Effects of multiple scattering on weather radars have been rarely studied in the remote sensing society. As an experimental demonstration, Ito et al. [1] pointed out that large linear depolarization ratios (LDR) measured in rains with 35 GHz radars can be attributed to multiple scattering effect rather than single scattering from non-spherical particles. Marzano et al. [2] simulated the multiple scattering effect for convective rains through a Monte-Carlo method, and reported that overestimation of reflectivity due to multiple scattering can reach nearly 20 dBZ. Recently, Kobayashi et al. [3] derived a theory of second order scattering for a radar with finite-beam width, and found that the reflectivity of second order scattering increases as a function of the ratio of footprint radius to mean free path of a random medium, and that this reflectivity asymptotically approaches the values that the plane-wave incident theory [4] predicts. Battaglia et al. [5], on the other hand, performed another Monte Carlo simulation in which the finite beam effect is explicitly taken into account. Their results, in good agreement with the theoretical prediction of Kobayashi et al., showed that the multiple scattering effect for a spaceborne radar can reach 10-20 dBZ at 35 GHz, while almost negligible for an airborne radar due to its small footprint size.

In this paper, the second order scattering approximation based on Ito et al. [6] is applied for W-band pulsed radars. A single layer of random medium is assumed to consist of spherical particles of uniform size. When considering a general particle distribution of spherical particles, a similar conclusion can be derived by taking ensemble average over an absorption coefficient and a scattering matrix. Furthermore, the method itself can be easily extended to higher order multiple scatterings, and also to multiple layers of hydrometeors. However, the formalism is based on the radiative transfer theory so that the solutions can not include the effects of cross terms, i.e. backscattering enhancement.

II. Formalism

Figure 1 is a schematic of a layer of hydrometeors of thickness d. A radar antenna at point A_n with a narrow 3-dB beam width $\theta_d \ll 1$ is located at a distance R from the top of the medium. The origin of position coordinate O is assumed to be set at the beam center on the surface. Suppose that the antenna A_n transmits a rectangular pulse of duration time T with a linear polarization. The origin of time t is set at the moment when the transmitted pulse reaches the top surface of the medium. Furthermore the transmitting and receiving antenna gains are assumed to be equal, denoted by G. z and $\boldsymbol{\rho}$ represent the longitudinal and transverse coordinates of an arbitrary point $\boldsymbol{x}$. The 3-dB footprint radius $\sigma_r(z)$ at z can be represented as

$$\sigma_r^2(z) \equiv \frac{(R+z)^2\theta_d^2}{8\,ln2} \tag{1}$$

When the medium consists of spherical particles, the specific intensity at point $\boldsymbol{x}$ in a general direction $\widehat{\Omega}$ is represented as a solution of time-dependent radiative transfer equation[1]:

$$\left(\frac{1}{c}\frac{\partial}{\partial t} + \widehat{\Omega}\cdot\frac{\partial}{\partial \boldsymbol{x}} + \kappa_e\right)\boldsymbol{J}(z,\boldsymbol{\rho},\widehat{\Omega},\,t) = \int d\widehat{\Omega}'\boldsymbol{\Psi}(\widehat{\Omega},\,\widehat{\Omega}')\boldsymbol{J}(z,\boldsymbol{\rho},\widehat{\Omega}',\,t) \tag{2}$$

where c is the speed of light. κ_e denotes the extinction rate given by the Foldy-Oguchi-Twelsky formula [7]. $\boldsymbol{\Psi}(\widehat{\Omega},\,\widehat{\Omega}')$ denotes the 4x4 scattering matrix of the medium. Notice that the coherent (reduced) specific intensity must satisfy the homogeneous part of Eq. 2. Once we determine an optimal form of coherent specific intensity, the first order specific intensity can be obtained by the perturbation technique as described in

the authours' companion paper. When the extinction rate from the top surface of medium to point A_n is represented by κ_{ar}, the intensity received by the antenna at time $t + R/c$ can be obtained by multiplying the receiving cross-section with the intensity aiming point A_n, followed by integration over solid angle. The result is written:

$$I_r^{(1)} = I_B R^2 \mathbf{\Phi}(\widehat{\Omega}_B, \widehat{\Omega}_I)\boldsymbol{I_0} \int_{max[c(T-t)/2,\,0]}^{min[ct/2,\,d]} \frac{e^{-2\kappa_e z'}}{(R+z')^2} dz' \tag{3}$$

where the constant I_B is defined as

$$I_B = \frac{\pi P_t G^2 \theta_d^2\, e^{-2\kappa_{ar} R}}{2^5 k^2 R^2 ln2} \tag{4}$$

The directions $\widehat{\Omega}_B$ and $\widehat{\Omega}_I$ are defined as

$$\widehat{\Omega}_B = (\pi, ^{\forall}\varphi_B) \tag{5}$$

$$\widehat{\Omega}_I = (0, ^{\forall}\varphi_I) \tag{6}$$

In a similar manner, the returned 4-d intensity for the second order scattering can be obtained as

$$\begin{aligned}
I_r^{(2)} \approx{}& \tfrac{\pi P_t G^2}{2k^2R^2} \int_0^{2\pi} d\Phi \int_0^{\infty} d\rho_0 \cdot \rho_0 \cdot exp[-\rho_0^2/(2\sigma_r^2(0)] \\
& \int_0^{2\pi} d\varphi' \int_0^{d} dz' e^{-\kappa_e z'} \{ \int_0^1 d\mu' \tfrac{1}{\mu'} \mathbf{\Phi}(\widehat{\Omega}_B, \widehat{\Omega}')\mathbf{\Phi}(\widehat{\Omega}', \widehat{\Omega}_i)\boldsymbol{I_0} \\
& \int_0^{z'} dz" \, exp[-\kappa_e z" - \tfrac{\kappa_e}{\mu'}(z' - z")] \tfrac{1}{(R+z")^2} \\
& \cdot exp[-\{\rho_0^2 - \tfrac{2(z'-z")}{\mu'}\rho_0(1-\mu'^2)^{1/2} cos\varphi' + \\
& \tfrac{1-\mu'^2}{\mu'^2}(z' - z")^2\}/(2\sigma_r^2(z"))] \\
& \cdot rect[t + \tfrac{z'}{c}(-1 - \tfrac{1}{\mu'}) + \tfrac{z"}{c}(\tfrac{1}{\mu'} - 1);\, 0,\, T] \\
& \int_{z'}^{d} dz" \, exp[-\kappa_e z" - \tfrac{\kappa_e}{\mu'}(z' - z")] \tfrac{1}{(R+z")^2} \\
& + \int_{-1}^{0} d\mu' \tfrac{1}{-\mu'} \mathbf{\Phi}(\widehat{\Omega}_B, \widehat{\Omega}')\mathbf{\Phi}(\widehat{\Omega}', \widehat{\Omega}_i)\boldsymbol{I_0} \\
& \cdot exp[-\{\rho_0^2 - \tfrac{2(z'-z")}{\mu'}\rho_0(1-\mu'^2)^{1/2} cos(\varphi' - \Phi) \\
& + \tfrac{1-\mu'^2}{\mu'^2}(z' - z")^2\}/(2\sigma_r^2(z"))] \\
& \cdot rect[t + \tfrac{z'}{c}(-1 - \tfrac{1}{\mu'}) + \tfrac{z"}{c}(\tfrac{1}{\mu'} - 1);\, 0,\, T]\}
\end{aligned} \tag{7}$$

where the variable ρ_0 has been introduced as $\rho_0 = R \cdot tan\Theta$.

III. Results and discussions

In this paper, a layer thickness d, a range resolution $cT/2$, and a footprint radius σ_r are normalized by the mean free path of medium l_{free}, and represented by τ_d, τ_p and Ξ_r respectively. For calculation of Fig. 2, a single layer of spherical water particles of uniform diameter $D = 1$ mm is assumed to have the normalized thickness $\tau_d = 2$ at temperature of 20°C. A pulse of the normalized range resolution $\tau_p = 0.1$ is incident with the normalized footprint radius $\Xi_r = \infty$. The carrier frequency in the pulse is set at 95 GHz. The return signals of the first and second order scattering at time $t+R/c$ are given by Eqs. 3 and 7, respectively. Without losing generality, we can eliminate the effect of distance R from the receiving time $t + R/c$, redefining the receiving time as t. Alternatively, we can represent the receiving time t by using the normalized range $\tau_r = 2^{-1}ct/l_{free}$. The normalized first order copolarized power-return l_1^{co} and cross-polarized power-return l_1^{cx} are defined by dividing Eq. 3 by Eq. 4. It is noticed that l_1^{cx} is always zero for the spherical particles. In a similar manner, the normalized second order copolarized power-return l_2^{co}, and cross-polarized power-return l_2^{cx} are defined. The normalized footprint radius $\Xi_r = \infty$ is first assumed for Fig. 2, which corresponds to the plane wave incidence theory [1]. In Fig. 2a, l_1^{co}, l_2^{co} and l_2^{cx} are plotted as functions of the normalized range τ_r. Figure 2b shows the linear depolarization ratio (LDR) defined by $l_2^{cx}/(l_1^{co} + l_2^{co})$. The abrupt increase in LDR from $\tau_r = 2$ to 2.1 can be explained by the vanishment of l_1^{co} at the rear edge of medium. LDR slowly approaches its second order asymptotic value of -6.5 dB that is calculated from Eq. (28) in [3]. To see the effect of a finite footprint radius, calculation is performed for $\tau_r \leq 2.6$ with a smaller normalized footprint radius $\Xi_r = 0.2$ and the other parameters kept the same as those in Fig. 3. It is noticed that the first order term l_1^{co} is invariant for change in Ξ_r. On the other hand, the values of l_2^{co} and l_2^{cx} in Fig. 3a become lower than those in Fig. 2a, and l_2^{co} becomes always lower than l_1^{co} in contrast to Fig. 2a, because the second order scatterings with scattering angles near $\theta' = 90°$ can not be effectively collected with such a small footprint. The rapid decreases of l_2^{co} and l_2^{cx} after $\tau_r = 2$ are conspicuous due to the same reason. LDR in Fig. 3b also shows great difference from that in Fig. 2b. The fast approach to the asymptotic value (-6.5 dB) is related to the aforementioned rapid decreases of l_2^{co} and l_2^{cx}.

In Fig. 4a, the second order power-returns l_2^{co} and l_2^{cx} for $\Xi_r = 0.2$ and ∞ are compared as functions of the normalized range τ_r. As τ_r increases, the difference between $\Xi_r = 0.2$ and ∞ increases. This feature is more serious in cross-polarized return than in copolarized return, because the contribution of scattering of $\theta' \approx 90°$ to the second order scattering is larger in cross polarization than in copolarization [3]. In Fig. 4b, l_1^{co}, l_2^{co} and l_2^{cx} are plotted as functions of the normalized footprint radius Ξ_r for fixed normalized ranges $\tau_r = 1.8$. As mentioned for Fig. 3, the first order term l_1^{co} is invariant for change in Ξ_r. The second order terms l_2^{co} and l_2^{cx} decrease strongly for $\Xi_r \lessapprox 1$. On the other hand, for $\Xi_r \gtrapprox 2$, these values asymptotically approach to the values predicted by the plane wave incidence case that is given by $\Xi_r = \infty$. When considering spaceborne radar operation such as in CloudSat Mission [8], [9], the deductions from Figs. 4 a and b imply that the multiple scattering effect must be taken into account due to its large footprint radius as also reported by [3], [5].

References

[1] Ito, S., T. Oguchi, T. Iguchi, and H. Kumagai, and R. Meneghini, "Depolarization of radar signals due to multiple scattering in rain," *IEEE Trans. Geosci. Remote Sensing*, vol. 33, pp. 1057-1062, 1995.

[2] Marzano, F., L. Roberti, S. D. Michele, A. Mugnai, and A. Tassa, "Modeling of apparent radar reflectivity due to convective clouds at attenuating wavelengths," *Radio Science*, vol. 38, 1002, doi:1029/2002RS002613, 2003.

[3] Kobayashi, S., S. Tanelli, and E. Im, "Second order multiple scattering theory associated with backscattering enhancement for a millimeter-wavelength weather radar with a finite beam width," *Radio Science*, vol. 40, RS6015, doi: 10.1029/2004RS003219, 2005.

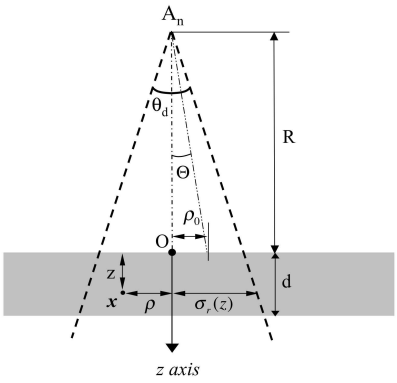

Fig. 1. A schematic of a layer of hydrometeors of thickness d. A radar antenna at point A_n with a narrow 3-dB beam width $\theta_d \ll 1$ is located with a distance R from the top of the medium. z and ρ are the longitudinal and transverse coordinates of an arbitrary point $\boldsymbol{x}$, while ρ_0 is defined as a function of Θ on the top surface. $\sigma_r(z)$ denotes the 3-dB footprint radius at z.

[4] Mandt, C.E., L. Tsang, and A. Ishimaru, "Copolarized and depolarized backscattering enhancement of random discrete scatterers of large size based on second-order ladder and cyclical theory," *J. Opt. Soc. Am. A.*,vol. 7, pp. 585-592, 1990.

[5] Battaglia, A, Ajewole, M.O. and Simmer, C., "Multiple scattering effects due to hydrometeors on precipitation radar systems," *Geophys. Res. Lett.*, vol. 32, L19801, doi:10.1029/2005GL023810, 2005.

[6] Ito, S., T. Oguchi, and S. Kobayashi, "Backscattering of millimeter waves from rain media: Effects of a finite beam width," *Proceedings of the 2005 IEICE Society Conference*, B-1-6, pp. 6, 2005.

[7] Oguchi, T., "Attenuation and phase rotation of radio waves due to rain: Calculations at 19.3 and 34.8 GHz," *Radio Science*, vol. 8, pp. 31-38, 1973.

[8] Im, E., C. Wu, and S.L. Durden, "Cloud profiling radar for the CloudSat Mission," *IEEE Aerospace and Electronic System Magazine*, vol. 20, pp. 15-18, 2005.

[9] Stephens, G.L., D.G. Vane, R.J. Boain, G.G. Mace, K. Sassen, Z. Wang, A.J. Illingworth, E.J. O'Connor, W.B.Rossow, S.L. Durden, S.D. Miller, R.T. Austin, A. Benedetti, C. Mitrescu, and the CloudSat science team, "The CloudSat Mission and the A-Train," *Bull. Amer. Meteor. Soc.*, vol. 83, pp. 1773-1789, 2002.

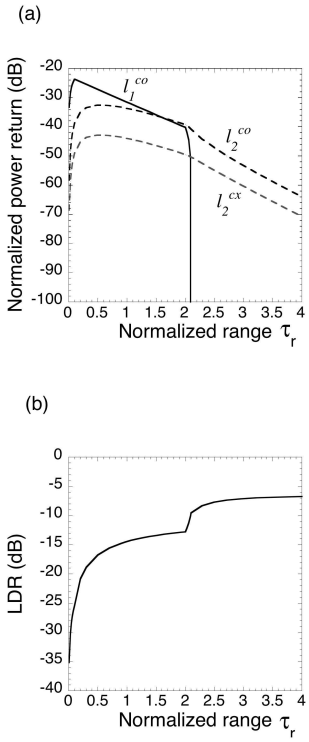

Fig. 2. Normalized footprint radius $\Xi_r = \infty$ is used for calculation. a): The normalized power-returns l_1^{co}, l_2^{co} and l_2^{cx} are plotted as functions of the normalized range τ_r. Note that l_1^{co} vanishes after $\tau_r = 2.1$. b): The linear depolarization ratio (LDR) versus the normalized range τ_r.

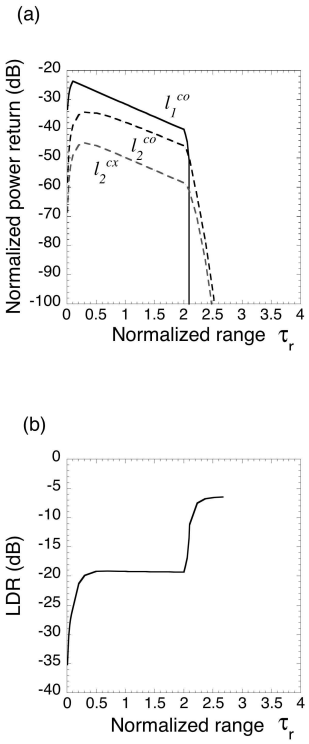

Fig. 3. Normalized footprint radius $\Xi_r = 0.2$ is used for calculation. The other parameters are kept the same as those in Fig. 2. a): l_1^{co}, l_2^{co} and l_2^{cx} are plotted as functions of the normalized range τ_r. b): LDR versus the normalized range τ_r.

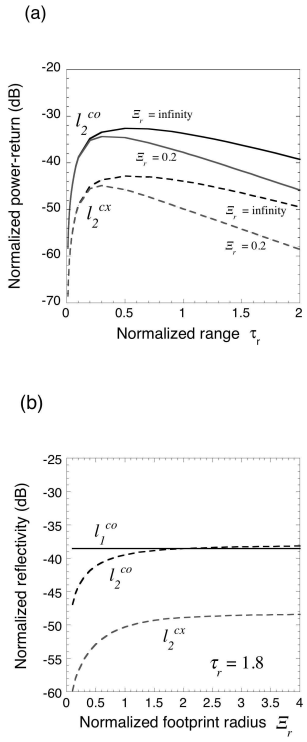

Fig. 4. a): The second order power-returns l_2^{co} and l_2^{cx} for $\Xi_r = \infty$ and $\Xi_r = 0.2$ are compared as functions of the normalized range τ_r. b): l_1^{co}, l_2^{co} and l_2^{cx} are plotted as functions of normalized footprint radius Ξ_r. The normalized range is set at $\tau_r = 1.8$. Note that l_1^{co} is invariant with Ξ_r. l_2^{co} and l_2^{cx} decrease strongly for $\Xi_r \lessapprox 1$, while these values asymptotically approach to the values predicted by Eq. 7 with $\Xi_r = \infty$.